MODE LOCALIZATION AND TUNABLE OVERLAP IN A CLOSED-CHAIN MICROMECHANICAL RESONATOR ARRAY

Joon Hyong Cho[1,2], Michael A. Cullinan[2] and Jason J. Gorman[1]
[1]National Institute of Standards and Technology, USA
[2]Walker Department of Mechanical Engineering, University of Texas at Austin, USA

ABSTRACT
In this paper, we explore the dynamics of a closed chain of coupled micromechanical resonators, where each resonator is coupled to its two nearest neighbors. The design of a three-resonator array that combines silicon cantilevers with piezoelectric actuation and electrostatic coupling is first introduced. The dynamic behavior of the array is then presented for two voltage schemes for coupling the resonators, demonstrating complex amplitude and frequency dependence that may be useful for sensing applications. Finally, it is shown that analog feedback can induce mode localization in the array and collapse two coupled modes into a single mode, which could provide high sensitivity to external perturbations.

KEYWORDS
Coupled resonators, mode localization, resonator array, piezoelectric.

INTRODUCTION
Coupled micromechanical resonators have received significant attention over the last decade for both their ability to enhance measurement sensitivity in sensors and to demonstrate complex nonlinear behavior that may be useful for both classical and quantum computing [1-12]. Mode localization in coupled resonators has in particular been shown to be a powerful approach for improving the precision of microelectromechanical (MEMS) sensors, where the relative vibration amplitudes between resonators are used to measure external perturbations [1,2]. Sensing examples include accelerometers [3] and mass sensors [4], but mode localization can be used to measure any external signal capable of altering individual resonance frequencies and mode shapes of the coupled resonators.

From a more fundamental perspective, coupled resonators have been used to demonstrate multi-mode avoided crossings, similar to behavior found in atomic systems [5]. Parametric resonance and amplification have also been explored in coupled resonators, resulting in nonlinear frequency conversion and classical dynamics that are analogous to Rabi oscillations found in two-level quantum systems [6]. Finally, coupled nonlinear dynamics have been shown to yield complex bifurcations that can drive oscillations across large arrays including more than 100 resonators [7] and generate phononic frequency combs with fixed frequency spacing around a parametric resonance [8]. Due to this wide range of applications for coupled resonators, there is a continued need to develop new resonator geometries that can better leverage the dynamic behaviors described above.

Many different actuation, sensing, and coupling mechanisms have been used to realize coupled resonator arrays. The combination of electrostatic actuation and capacitive sensing have been the most commonly employed combination [1,3,4], but piezoelectric materials have also been used for actuation and sensing [6,8], often with greater sensitivity. Resonator coupling methods have largely been limited to mechanical coupling, such as a flexural linkage, and electrostatic coupling, which provides continuous tunability. The topology for the majority of coupled resonator arrays has been confined to series connectivity, where each resonator is coupled to the next resonator in a linear chain,

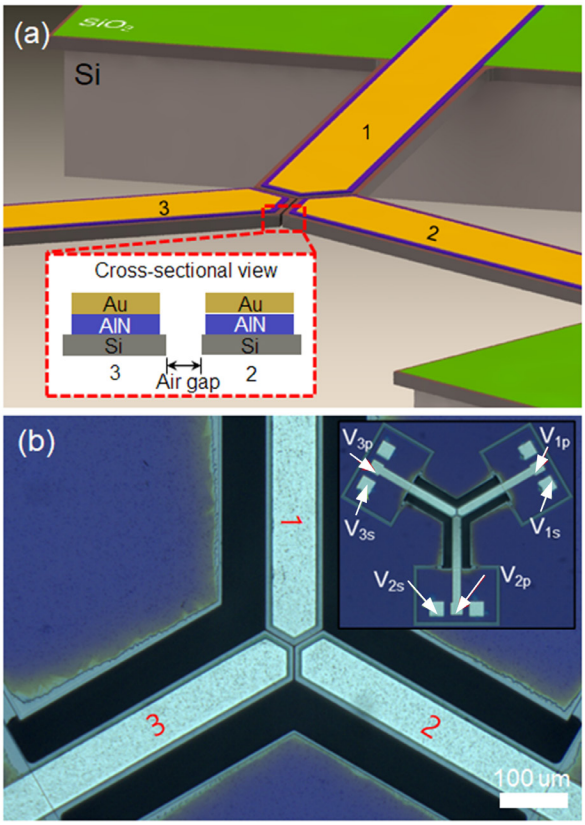

Figure 1: (a) Diagram of a 3-resonator closed-chain array. Inset: Cross-section of device layers. (b) Optical micrograph of a fabricated array. Inset: Electrical connections for the drive and coupling voltages.

with a few exceptions [9-11].

Here, we present a new design for resonator arrays that combines piezoelectric actuation and sensing with electrostatic coupling. This results in large vibration amplitudes that are transduced with high sensitivity while also having continuous coupling tunability. In addition, the array is coupled in a closed chain rather than a linear chain, where the last resonator in the chain is coupled back to the first resonator, as described in the next section. As a demonstration of the dynamic behavior of this array, two complementary schemes for tuning the coupling are implemented and the resulting amplitude and resonance frequency behaviors are presented. Finally, feedback control on an individual resonator is shown to be an effective approach for inducing mode localization and may be useful for optimizing the array's sensitivity to external perturbations.

RESONATOR ARRAY DESIGN
The design of the closed-chain coupled resonator array is shown in Fig. 1. The array is composed of three cantilever resonators that are connected to the substrate at the base and coupled to each other at their free ends. The cantilevers have three material layers: a

single-crystal silicon layer that is the primary structural element, an aluminum nitride (AlN) layer for piezoelectric actuation and sensing, and a gold layer for electrical contact. A sinusoidal drive voltage with tunable frequency is applied to the gold layer to actuate the cantilever (see Fig. 1b inset, V_{1p}, V_{2p}, and V_{3p}). The tips for all cantilevers come together in the center of the array, where they are separated by a gap in the silicon layer. The coupling between each resonator is controlled by setting the DC voltage on the silicon layer for each resonator, V_{1s}, V_{2s}, and V_{3s}, respectively (see Fig. 1b inset). In general, the electrostatic force between two cantilevers is highly nonlinear with respect to the relative heights of the cantilever tips compared to the substrate plane. However, for small cantilever displacements, the electrostatic force is a linear restoring force that results in a positive increase in stiffness. The combination of the three drive voltages and three coupling voltages provide a number of options for generating unique dynamic behavior. This closed-chain concept has previously been explored theoretically [9] and a closed chain of mechanically coupled tuning fork resonators has been presented previously [10]. However, to our knowledge, resonators with tunable electrostatic coupling in a closed chain has not been demonstrated experimentally to date.

A functional array is shown in Fig. 1b, which was fabricated using the MEMSCAP PiezoMUMPS multi-project wafer process [13]. The silicon layer has the <100> crystal plane oriented out of the plane of the substrate and is 10 µm thick, the AlN layer is 0.5 µm thick, and the electrostatic gap between resonators is 2 µm wide, which is the minimum dimension allowed for the process. Custom fabrication of the array would allow for further optimization of the electrostatic coupling, and the stiffness and resonance frequencies of the resonators.

RESULTS AND DISCUSSION

To demonstrate some of the linear dynamic behaviors attainable with the closed-chain coupled resonator array, we explored two schemes for tuning the electrostatic coupling while driving a single resonator. A homodyne laser interferometer was used to measure the out-of-plane resonator motion in all presented results, where the photodetector voltage is used for resonator amplitude rather than converting to displacement. All measurements were performed under ambient conditions.

In the first coupling scheme, resonator 3 was driven with a sinusoidal (AC) signal, V_{3p}, and was biased with a static DC voltage, V_{3s}, set to 15 V while the electrostatic interactions between the three resonators were tuned with bias voltages V_{1s} and V_{2s} on resonators 1 and 2, respectively (see Fig. 2a). The frequency response of resonator 2 was measured with the interferometer over a frequency range that captures the first three modes of the array and for a range of values for V_{1s} and V_{2s}. A representative frequency response, including amplitude and phase, is shown in Fig. 2b, where the 2nd and 3rd modes are visible. These modes are largely due to resonators 2 and 3, although they are somewhat shifted from those found for the uncoupled resonators. These two resonators should have nearly the same Young's modulus along their length due to their orientation in the silicon layer, resulting in similar resonance frequencies. The 1st mode is only barely detectable near 77 kHz in Fig. 2b. This mode is downshifted from the other two since resonator 1 sits in a different crystal plane.

The amplitudes for modes 2 and 3 for varying V_{1s} and V_{2s} are shown in Figs. 3a and 3c, respectively. Since the array is driven at resonator 3 and measured at resonator 2, only V_{2s} has an effect on amplitude, where it acts like a gain between the input and output signals. However, the electrostatic coupling has a more interesting effect on the resonance frequencies. As V_{1s} changes from positive to negative, the electrostatic coupling increases between resonators

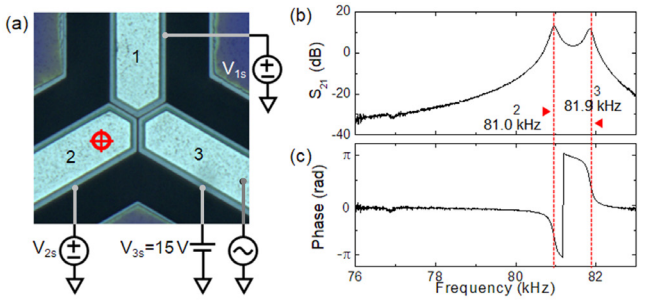

Figure 2: (a) First coupling scheme for the array. Resonator 3 is driven with an AC signal while a 15 V bias voltage is applied to its silicon layer. Varying bias voltages are applied on the silicon layers of resonators 1 and 2. (b) Representative amplitude and c) phase responses measured on resonator 2 with the interferometer (location indicated by the red cross in (a)). V_{1s} = 0 V, V_{2s} = 0 V.

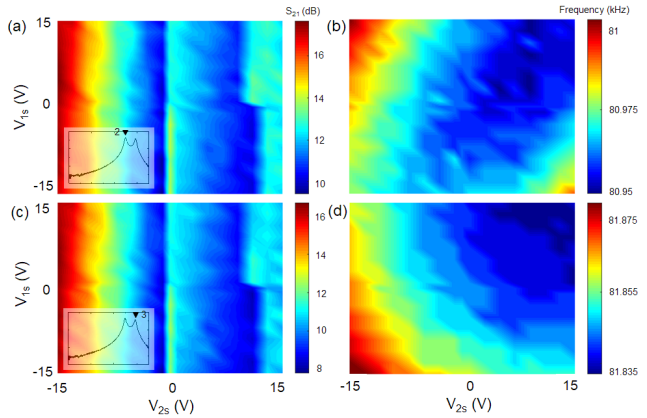

Figure 3: Experimental results for the coupling scheme in Fig. 2. (a) Amplitude and (b) frequency of mode 2. (c) Amplitude and (d) frequency of mode 3. V_{1s} has no effect on amplitude but tunes the frequencies of modes 2 and 3 in opposite directions. V_{2s} tunes both the amplitudes and frequencies for both modes in the same direction. Periodic artifacts in contour maps are computational and not representative of the data.

1 and 3 and decreases between resonators 1 and 2. Therefore, the frequencies for modes 2 and 3 are detuned in opposite directions and are a nonlinear function of the two bias voltages, as indicated by the semi-circular pattern shown in Figs. 3b and 3d. This behavior could provide a useful sensing modality where perturbations of resonator 1 can be transduced by measuring the frequency difference between modes 2 and 3. Examples of measurable perturbations include in-plane motion of resonator 1 and an induced voltage at V_{1s}, similar to voltmeters based on mode localization [14]. Since this is a differential frequency measurement between modes 2 and 3, it may be insensitive to thermal drift in the Young's modulus and coefficient of thermal expansion.

In the second coupling scheme, the coupling between resonators 1 and 2 was set to zero by choosing $V_{1s} = V_{2s}$ while V_{2s} and V_{3s} were varied (see Fig. 4a). A representative frequency response is shown in Fig. 4b, where the 1st mode is more pronounced than in the first scheme. This coupling scheme resulted in more linear behavior for the modal amplitudes and frequencies, as indicated by the linear gradients going from zero voltage to maximum voltage in the contour maps in Fig. 5. While this behavior is not particularly interesting on its own, it does point to the range of behaviors that can be achieved through small changes

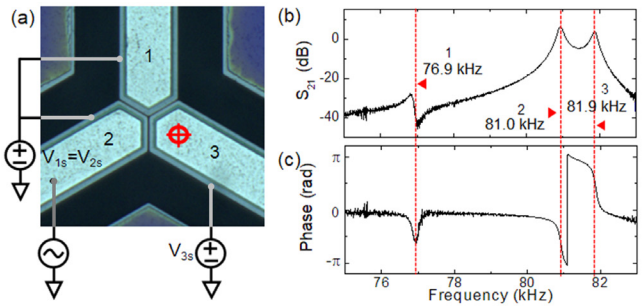

Figure 4: (a) Second coupling scheme for the array. Resonator 2 is driven with an AC signal while the same bias voltage is applied to the silicon layers of resonators 1 and 2. An independent voltage is applied to resonator 3. (b) Representative amplitude and c) phase responses measured on resonator 3 with the interferometer (location indicated by the red cross in (a)). V_{1s} = 0 V, V_{2s} = 0 V.

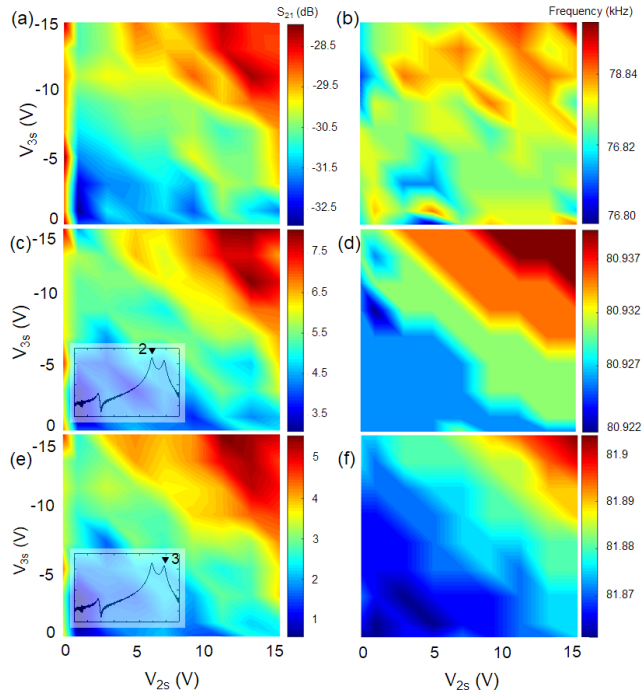

Figure 5: Experimental results for the coupling scheme in Fig. 4. (a,c,e) Amplitude and (b,d,f) frequency for modes 1, 2 and 3, respectively.

to the coupling configuration, as indicated by the dramatic differences in the array dynamics when comparing Figs. 3 and 5. This may be useful for creating mechanical logic gates used in low-bandwidth computation, where the coupling voltages, V_{1s}, V_{2s}, and V_{3s}, would be inputs to the logic gate and the resulting modal amplitude or frequency change would provide the computational output.

Finally, we used the same coupling scheme shown in Fig. 4a to explore the use of feedback control on an individual resonator to induce mode localization. We applied a negative stiffness perturbation to resonator 3, as is often done in mode localization sensors. However, rather than using a passive electromechanical element, such as an electrostatic actuator, analog proportional control was applied, where the interferometer signal was the feedback signal used to reduce the stiffness of the resonator. As seen in Fig. 6, mode 3 is reduced in frequency for increasing proportional gain until modes 2 and 3 collapse into a single mode

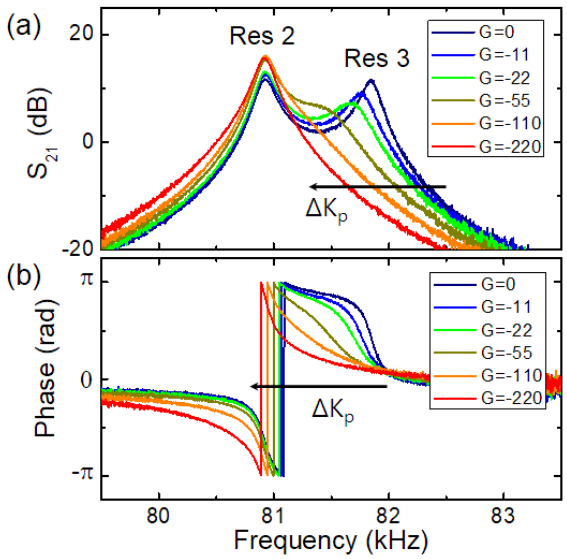

Figure 6: Modal overlap tuning with an analog proportional controller applied to resonator 3. (a) Amplitude and (b) phase of resonator 3 for varying proportional gain, which reduces the resonator stiffness. V_{2s} = 15 V, V_{3s} = -15 V.

that goes through a 2π phase shift on resonance. Similar overlapping modes generated by electrostatic coupling have recently been shown to be highly sensitive to external perturbations by operating in the weak coupling regime [12]. Here, the feedback reduces the stiffness of resonator 3 without changing the coupling between the resonators, thereby causing the modes to overlap. The impact of this feedback approach on the sensitivity of the array to stiffness perturbations on resonator 3 is currently being investigated.

CONCLUSION

A new topology for coupled resonator arrays has been presented that uses a closed chain of piezoelectric cantilevers that are electrostatically coupled at their free ends. Two sets of experiments with different voltage tuning rules for electrostatic coupling show that the dynamic behavior of the array can change dramatically based on the relative coupling forces. Finally, we have demonstrated that feedback control can be used to modify the coupling in the array, which may be useful for optimizing the sensitivity of the array to external perturbations. Future research will focus on expanding these early experiments to better understand the collective dynamics and applying the array to sensing applications.

REFERENCES

[1] P. Thiruvenkatanathan, J. Yan, J. Woodhouse, and A.A. Seshia, "Enhancing Parametric Sensitivity in Electrically Coupled MEMS Resonators," *J. Microelectromech. Sys.* **18**, 1077–1086 (2009).

[2] C. Zhao et al., "A review on coupled MEMS resonators for sensing applications utilizing mode localization," *Sens. Actuators A Phys.* **249**, 93–111 (2016).

[3] Y. Wang et al., "A mass sensor based on 3-DOF mode localized coupled resonator under atmospheric pressure," *Sens. Actuators A Phys.* **279**, 254-262 (2018).

[4] H. Zhang et al., "Mode-localized accelerometer in the nonlinear Duffing regime with 75 ng bias instability and 95 ng/√Hz noise floor," *Microsyst. Nanoeng.* **8**, 17 (2022).

[5] K. Gajo, S. Schüz, and E.M. Weig, "Strong 4-mode coupling of nanomechanical string resonators," *Appl. Phys. Lett.* **111**, 133109 (2017).
[6] H. Okamoto et al., "Coherent phonon manipulation in coupled mechanical resonators," *Nat. Phys.* **9**, 480–484 (2013).
[7] C.B. Wallin et al., "Nondegenerate parametric resonance in large ensembles of coupled micromechanical cantilevers with varying natural frequencies," *Phys. Rev. Lett.* **121**, 264301 (2018).
[8] A. Ganesan, C. Do, and A. Seshia, "Excitation of coupled phononic frequency combs via two-mode parametric three-wave mixing," *Phys. Rev. A 97*, 014302 (2018).
[9] V.B. Chivukula and J.F. Rhoads, "Microelectromechanical bandpass filters based on cyclic coupling architectures," *J. Sound Vib.* **329**, 4313–4332 (2010).
[10] A. Erbes, P. Thiruvenkatanathan, J. Yan, and A. A. Seshia, "Investigating vibration dynamics of cross-coupled MEMS resonators for reduced motional resistance," Transducers & Eurosensors XXVII, Barcelona (2013), pp. 1711–1714.
[11] B. Peng et al., "A sensitivity tunable accelerometer based on series-parallel electromechanically coupled resonators using mode localization," *J. Microelectromech. Sys.* **29**, 3–13 (2020).
[12] H. Zhang et. al, "On weakly coupled resonant MEMS transducers operating in the modal overlap regime," *IEEE Trans. Ultrason. Ferroelectr. Freq Control* **68**, 1448–1457 (2021).
[13] Certain commercial equipment, instruments, or materials are identified in this paper in order to specify the experimental procedure adequately. Such identification is not intended to imply recommendation or endorsement by NIST, nor is it intended to imply that the materials or equipment identified are necessarily the best available for the purpose.
[14] Y. Hao et al., "A micromechanical mode-localized voltmeter," *IEEE Sens. J.* **21**, 4325–4332 (2021).

CONTACT

*J.J. Gorman, tel: +1-301-975-3446; gorman@nist.gov